An Alternative Poincaré Section for Steady-State Responses and Bifurcations of a Duffing-Van der Pol Oscillator

Jang-Der Jeng[1], Yuan Kang[2*], Yeon-Pun Chang[2]
[1]Department of Mechanical Engineering, National United University, Taiwan, R.O.C.
[2]Department of Mechanical Engineering, Chung Yuan Christian University, Taiwan, R.O.C.
*Corresponding author: yk@cycu.edu.tw

Abstract: - To apply effective methods to analyze and distinguish all kinds of response patterns is an important issue of nonlinear dynamics. This paper contributes to develop an alternative Poincaré section method to analyze and identify the whirl responses of a nonlinear oscillator. This integration for analyzing high-order harmonic and chaotic motions is used to integrate the distance between state trajectory and the origin in the phase plane during a specific period. This response integration process is based on the fact that the integration value would be constant if the integration interval is equal to the response period. It provides a quantitative characterization of system responses as the role of the traditional stroboscopic technique (Poincaré section method) to observe bifurcations and chaos of the nonlinear oscillators. However, due to the signal response contamination of system, the section points on Poincaré maps might be too close to distinguish, especially for a high-order subharmonic vibration. Combining the capability of precisely identifying period and constructing bifurcation diagrams, the advantages of the proposed method are shown by the simulations of a Duffing-Van der Pol oscillator. The simulation results show that the high-order subharmonic and chaotic responses and their bifurcations can be effectively observed.

Key-Words: - Poincaré section method, Chaotic motion, Response integration, Bifurcation, Duffing-Van der Pol oscillator

1 Introduction

In recent twenty years, the problem of identifying and controlling chaos has become a hot topic in the field of physics, mechanics, engineering and other applied fields [1-7]. Because of the sensitivity of chaos to the system parameters and the initial value, identifying and controlling chaos has become important for nonlinear system. A strongly nonlinear system often exhibits a very complicated phenomenon including not only the periodic motion but also the quasi-periodic and chaotic motions. The identification of the aforementioned nonlinear behaviors is usually accomplished through the observation on bifurcation diagrams in terms of Poincaré section points with assistance of phase plane trajectories. Typical examples of the driven nonlinear oscillators are the Duffing oscillator and Van der Pol oscillator. The efforts for searching a better numerical method for nonlinear system have never ceased.

The forced Duffing and Van der Pol oscillators, which are known to describe many important oscillating phenomena in nonlinear engineering systems, has been investigated extensively in the past decade [8-15]. Much work has already been done to investigate the characteristics of Duffing or Van der Pol oscillator [8, 11, 15]. Stability and Bifurcation studies have been carried out, for example, by Duffing oscillator [14, 15] and Van der Pol oscillator [8, 10]. Numerical investigations have provided examples of period doubling bifurcations, and chaotic attractors [10, 13, 14, 15].

In applying the incremental harmonic balance method, with the focus on a Duffing oscillator with zero linear stiffness, Leung and Fung [2] discussed the variation in the bifurcation points according to the system's parametric changes and the boundaries of steady solutions of the system in 1989. In 1987, Parlitz and Lauterborn [8] used winding numbers to describe the dynamic behavior of the Van der Pol oscillator within the system and went on to explain its relationship to the system parameters. In 1996, Dooren and Janssen [9] had studied a Duffing oscillator under static and large periodic excitation by using the shooting method combined with the Newton method. They found that there are at least six cascades of period doubling subharmonic solutions in the amplitude of the periodic excitation fixed at specific values from bifurcation diagram. In 1996, Xu and Jiang [10] also investigated the global bifurcation characteristics of the forced Van der Pol oscillator.

In 2000, Kim et al. [17] experimentally investigated the dynamic stabilization in a double-well Duffing oscillator. They found that as the amplitude of driving force increases through a threshold value, the unstable symmetric orbit was found to become stable via a reverse supercritical pitchfork bifurcation by absorbing a pair of stable symmetric orbits. In 2004, a chaotic crisis in forced Duffing oscillators had been investigated by Hong and Xu [14] using the generalized cell mapping digraph method analyzed nonlinear system. They examined that the chaotic attractor together with its basin of attraction is suddenly destroyed as the parameter passes through the critical value, and the chaotic saddle also undergoes an abrupt enlargement in its size. However, such a detailed model is not always the most suitable approach if the main aim is to obtain efficient predictions of overall system dynamics.

The intensive studies by many researchers have revealed many characteristics of the oscillators. However, it is still a difficult task to identify quantitatively for the high-order of harmonic responses due to the signal contamination of system response. However, an effective method for analyzing the high-order harmonic and chaotic motions in a Duffing-Van der Pol system has not been sufficiently investigated. For this purpose we propose a response integration method to analyze high-order harmonic and chaotic motions in the nonlinear models of periodically forced Duffing-Van der Pol oscillator. This study contributes to the development of efficient integration method to analyze and identify the whirl responses of a nonlinear system. This integration method provides a quantitative characterization of periodic motion. It is a useful tool to observe the periodic motion which generally cannot be easily distinguished from either the orbit plot or the Poincaré map. It is shown that this method provides valuable information in bifurcation diagram such that the parameter range leading to chaos can be easily decided and the number of distinguishable time-domain responses can be determined. Since this method can filter combination and distinguish response pattern. Some examples are given to illustrate its effectiveness and convenience.

2 Method of response integration algorithm

The nonlinear, non-autonomous systems can be expressed in a nondimensional form of the first-order differential equation as follows:

$$\frac{d\tilde{x}}{dt} = f(\tilde{x}, t), \tag{1}$$

where $\tilde{x} \in R^n$ is the n-dimensional vector of nondimensional variables ; $t \in R$ is a nondimensional time.

An integration algorithm denoted by P_{nT} integration which was defined by integrating integrand function and expressed by

$$P_{nT}(t_c) = \int_{t_c}^{t_c+nT} f(x, \dot{x})\, d\, t \tag{2}$$

where the integrand function can be presented by $f(x, \dot{x}) = x(t)$, $\dot{x}(t)$ or $\sqrt{x^2(t) + \dot{x}^2(t)}$.

The integrand represents the distance between trajectories and origin or trajectories and one of the coordinate axes in phase plane. $x(t)$ and $\dot{x}(t)$ are time histories of nondimensional displacement and velocity, respectively. t is nondimensional time and, t_c is an arbitrary time for nondimensional parameters, taken at the time of steady-state. It is a changing index which is helpful to distinguish the system's response period. The T is the period of single excitation or the smallest common multiple period of multiple excitations. The integration interval nT is set to be the predicted oscillating period. Constant P_T can be obtained from time history, when response is P-1 motion. Therefore, when the integration interval is set at nT (n is an integer larger than zero), it can be judged that the system periodic response is P-n motion, that is, the n-*th* is a subharmonic response. Moreover, if the integration interval is set as the excitation period, i.e., T , the results can be used to draw the bifurcation diagram of the rotor system. The extraction period is the same as Poincaré section method.

When the period of n-*th* order subharmonic motion is nT , the steady state response has

$$f(x, \dot{x}) = f(x(t+nT), \dot{x}(t+nT)) \tag{3}$$

Thus, integration P_{nT} of $f(x, \dot{x})$ differentiating to time t_c gives

$$\frac{dP_{nT}(t_c)}{dt_c} = f(x(t_c+nT), \dot{x}(t_c+nT)) - f(x(t_c), \dot{x}(t_c)) = 0 \tag{4}$$

Therefore,

$$P_{nT}(t_c) = constant \tag{5}$$

$$\text{or} \quad \Delta P_{nT} = P_{nT}(t_c+1) - P_{nT}(t_c) = 0 \tag{6}$$

The method to differentiate the system responses with the response integration is based on the relations among extraction time t_c and integration interval nT . The analytical process of response integration is as the following:

1. First, an initial value n is given and the integration interval is set as nT where n is an integer and T is the excitation period of system. Furthermore, t_c will be varied to assist in the determination of the response period.
2. The ΔP_{nT} integration versus t_c are calculated, and the $t_c - \Delta P_{nT}$ curve is drawn. If the integration ΔP_{nT} is not zero, then the index n should be changed, and the above steps are repeated.
3. When the integration ΔP_{nT} is zero, the integration interval nT is defined as n times of excitation period; the system response is P-n periodic motion, i.e., n -order sub-harmonic vibration. If the index n is changed constantly, no fixed integration value can be obtained, and the system response might be chaotic motion.

As proof of the above for periodic motion, see Eq. (5) with period nT the integral P_{nT} is constant against the starting time of integration. Thus, the period nT of a steady state response can be identified due to the existence of constant P_{nT}. Moreover, the Poincaré section method requires more sampling numbers to eliminate the measurement noise. Based on the definition described as above, the response period which determined to apply the response integration method needs only to be within the time range. The extraction time range can be an arbitrarily small number. Therefore, when limited experimental measurement data are analyzed, it is more advantageous to use the response integration method.

3 Simulation results and analysis

3.1 Duffing-Van der Pol oscillator

The representative nonlinear oscillator subjected to driving periodic force, evolved from mechanical system illustrated in Fig. 1, are considered as examples herein to demonstrate the usage and effectiveness of the proposed response integration method. The nonlinear oscillator used in this paper is from the Duffing-Van der Pol equation. The oscillator can be used to model rotor subjected to nonlinear damping and stiffness with external excitation. The Duffing-Van der Pol oscillator is one of the most common types of nonlinear oscillators and has many typical nonlinear phenomena [13, 18]. The governing differential equation of the nonlinear system can be written as

$$m\ddot{x} + c_1(c_2 - c_3x^2)\dot{x} + k_1x + k_2x^3 + k_3x^5 = f\cos(\omega t) \tag{7}$$

where m denotes the mass of the system; c_1, c_2 and c_3 denote damping coefficients respectively; k_1, k_2 and k_3 denote the stiffness coefficients respectively due to material nonlinearity; f denotes the amplitude of the external harmonic force; ω denotes the whirling frequency. These parameters also control the nonlinearity of the oscillator. The dot denotes a differentiation with respect to time t. It is assumed that the above system parameters are dimensionless in the Duffing-Van der Pol equation. For $m = 1$ and $c_3 = 0$, Eq. (7) is a famous Duffing equation. For $m = 1$, $c_1 = 0$, $k_2 = k_3 = 0$, Eq. (7) is a famous Van der Pol equation.

For performing numerical integration, the system equations are transformed into first-order form by introducing two variables x_1 and x_2.

$$\begin{aligned} \dot{x}_1 &= x_2 \\ \dot{x}_2 &= \frac{1}{m}\{-c_1(c_2 - c_3x_1^2)x_2 - k_1x_1 - k_2x_1^3 - k_3x_1^5 \\ &\quad + f\cos(\omega t + \phi)\} \end{aligned} \tag{8}$$

It is difficult to obtain the exact solutions directly. For this reason, the numerical simulations are performed by employing a fourth-order Runge-Kutta algorithm and a smaller integration step are chosen to be smaller than $\Delta t = 2\pi/200$ to ensure a steady-state solution.

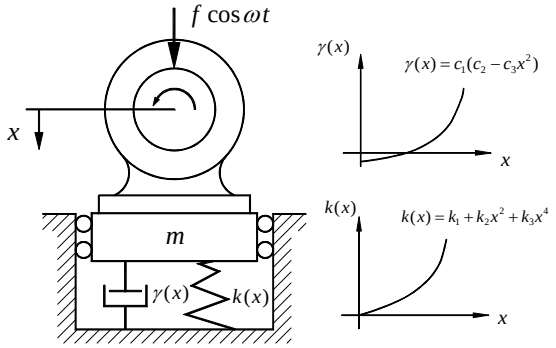

Fig. 1. Duffing-Van der Pol oscillator model for rotor excitation.

3.2 P_T integration bifurcation diagram analysis

The bifurcation diagram is a very effective mean to reflect the motion change; the results obtained from the system exhibiting of non-linear behaviors may be presented. As mentioned earlier, an integration

algorithm denoted by P_{nT} integration which was defined by integrating integrand function. The integrand function can be presented by $f(x,\dot{x}) = x(t)$, $\dot{x}(t)$ or $\sqrt{x^2(t)+\dot{x}^2(t)}$. To examine the system responses of the Duffing-Van der Pol oscillator compared with different integrand functions have been devised. The bifurcation diagrams with different integrand functions are shown in Figs. 2(a), 2(b) and 2(c). The bifurcation responses are calculated an increment $\Delta f = 4.286\times10^{-4}$ as the variation of the control parameter f. The forcing amplitude of the periodic excitation ranges from $f = 1.95$ to $f = 2.25$. As observed from these figures, the results show that the period doubling bifurcations and chaotic output responses in bifurcation diagram exhibit the similar forms of vibration. Our simulations in Fig. 2(c) show that the chaotic output responses have the larger scale in comparison with other two cases. Based on above results, in this paper we choose $f(x,\dot{x}) = \sqrt{x^2(t)+\dot{x}^2(t)}$ as the integrand function.

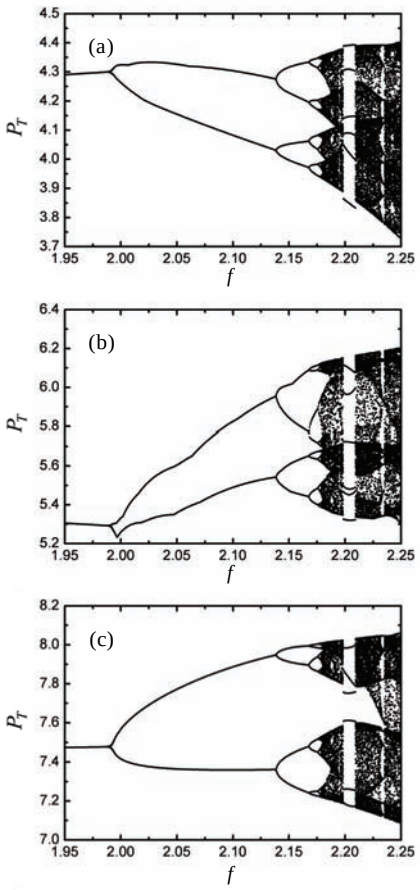

Fig. 2 Bifurcation diagrams with different integrand functions, (a) $f(x,\dot{x}) = x(t)$, (b) $f(x,\dot{x}) = \dot{x}(t)$, (c) $f(x,\dot{x}) = \sqrt{x^2(t)+\dot{x}^2(t)}$; $m = 1$, $c_1 = 0.47$, $c_2 = 1.0$, $c_3 = 1.0$, $k_1 = -1.07$, $k_2 = 3.48$, $k_3 = 1.14$, $\omega = 1.0$.

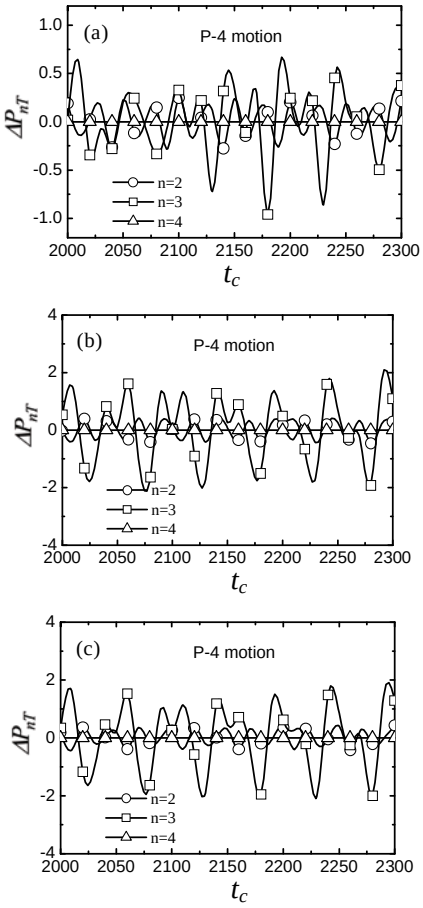

Fig. 3 Plots of ΔP_{nT} integration with different integrand functions, (a) $f(x,\dot{x}) = x(t)$, (b) $f(x,\dot{x}) = \dot{x}(t)$, (c) $f(x,\dot{x}) = \sqrt{x^2(t)+\dot{x}^2(t)}$. $m = 1$, $c_1 = 0.47$, $c_2 = 1.0$, $c_3 = 1.0$, $k_1 = -1.07$, $k_2 = 3.48$, $k_3 = 1.14$, $\omega = 1.0$, $f = 2.15$.

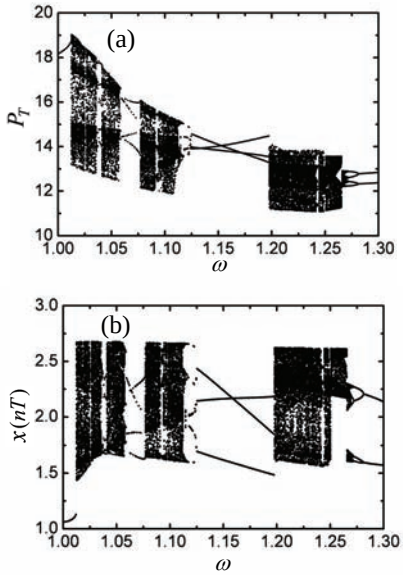

Fig. 4 Bifurcation diagrams with whirling frequency, ω as the control parameter, (a) the response integration method; (b) Poincaré section method; with

$c_1 = 0.15$, $c_2 = 1.0$, $c_3 = -0.8$, $k_1 = 0.05$, $k_2 = 0.65$, $k_3 = 0.26$, $\omega = 1.6$.

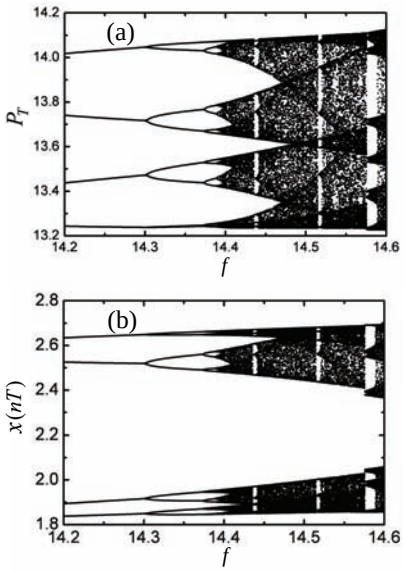

Fig. 5 Bifurcation diagrams with forcing amplitude, f as the control parameter, (a) the response integration method; (b) Poincaré section method.

The plots of ΔP_{nT} integration with different integrand functions as shown in Figs. 3(a), 2(b) and 2(c) are also the same results. In order to validate the analysis results from the Response integration method, comparisons are made with Poincaré section method. Figs. 4(a) and 4(b) are the bifurcation diagrams drawn with both the response integration method and the Poincaré section method, using the whirling frequency as the control parameters. The whirling frequency ω ranges from 1.0 to 1.3 with a step of 0.0005. In these calculations, we choose the parameters as $m = 1$, $c_1 = 0.35$, $c_2 = -1.0$, $c_3 = -1.0$, $k_1 = 0.15$, $k_2 = 0.65$, $k_3 = 0.26$, $f = 7.8$. Similarly, the present method is evaluated by a comparison with Poincaré section method to show the excellent agreement. It can be seen that the motion is synchronous with period-one from 1.0 to 1.012, only one point is correspondingly shown in the bifurcation diagram for every whirling frequency. As the whirling frequency continues to increase, the motion suddenly goes into chaotic region from about $\omega = 1.012$. When ω increases further, at $\omega = 1.116$, the response goes out of chaos and turns to period-three motion. Then, with further variations of ω, the response again goes to chaos at $\omega = 1.198$. When $\omega = 1.272$, the response exits chaos and turns into period doubling bifurcations. Comparisons of the response bifurcations drawn with two methods are shown in Figs. 5(a) and 5(b). The bifurcation responses were calculated as the variation of the control parameter f. The forcing amplitude of the periodic excitation ranges from $f = 14.2$ to $f = 14.6$. The response integration method is evaluated by a comparison with the Poincaré section method to show the excellent agreement with the same set of parameters as in Figs. 5(a) and 5(b). It can be seen that the bifurcations of the Poincaré section and the response integration methods almost show the same topology of the structure for the same system parameters. The bifurcation diagram shows that period doubling bifurcations initially occurs. For the values of ranging from $f = 14.2$ to $f = 14.39$, the period doubling bifurcations are found to proceed in these figures. The chaos occurs after the period-four, period-eight, suddenly and then, bifurcates to period-sixteen. Herein, the period doubling bifurcation plays an important role in the occurrence of chaotic attractors. As the f continues to increase; the motion gradually enters into the region of chaos which remains from 14.39 to 14.6. Nevertheless, it is sometimes difficult to identify the period doubling bifurcation of system using the Poincaré section method to strobe Poincaré section points in Fig. 5(b). Conversely, when the response integration method is used, the period doubling bifurcation characteristics can clearly be observed in the bifurcation diagram shown in Fig. 5(a). It can be seen that the system exhibits very rich forms of periodic and chaotic vibrations.

3.3 Comparisons with response integration and the Poincaré section methods

The Poincaré section is a stroboscopic picture of a motion and consists of the time series at a constant interval of T, with T being the period of excitation. The corresponding Poincaré map is a combination of those return points and these discrete points are often called an attractor. Examination of the distribution of return points on the Poincaré map can reveal the response of motion. In case of a periodic motion, the *n* discrete points on the Poincaré map indicate that the period of motion is the P-n. For a chaotic motion, the return points form a geometrically fractal structure.

Figs. 6-10 show the plots of ΔP_{nT} integration and the Poincaré map with various forcing amplitudes. In these calculations, we choose the parameters as $m = 1$, $c_1 = 0.15$, $c_2 = 1.0$, $c_3 = -0.8$, $k_1 = 0.05$, $k_2 = 0.65$, $k_3 = 0.26$, $\omega = 1.6$. In the analysis of the Poincaré section method, the extraction time

equals to the external excitation period of $T = 2\pi/\omega$. When $f = 14.2$, Fig. 6(a) shows ΔP_{nT} integration value versus t_c with integration duration. The ΔP_{nT} integration value appears zero as continuously varying t_c at $n = 4$. This figure clearly illustrates the system response to be a period-four motion. At this time, the motion is a periodic motion and there is four points in the Poincaré map as shown in Fig. 6(b). At $f = 14.35$, due to a few Poincaré section points being too close, that is, the contamination of the signal response, thus it is difficult to identify the order of the subharmonic motion as shown in Fig. 7(b). But from Fig. 7(a), the plot of ΔP_{nT} integration, we can differentiate the motion clearly to be a subharmonic motion with period-eight. Similarly, at $f = 14.38$ it is also difficult to identify periodic responses; this is due to some Poincaré section points being too close. Details are as shown in Fig. 8(b). But what we can easily observe is that the motion is a sub-harmonic vibration with period-sixteen. As f are increased to 14.45 and 14.55, it is found that the ΔP_{nT} integration values never keep zero as continuously varying t_c even with the integration interval set very large as shown in Figs. 9(a) and 10(a). It indicates that responses are not periodic motions. The results of the Poincaré section method also show the responses to be chaotic motions as shown in Figs. 9(b) and 10(b). It can be seen that a period doubling route to chaos for a selection of f when another system parameters are fixed. The Duffing-Van der Pol system also represents the complex dynamic characters at different forcing amplitudes obviously.

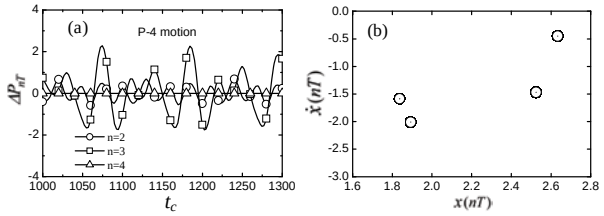

Fig. 6 Plots of ΔP_{nT} integration (left) and Poincaré map (right) with $f = 14.2$.

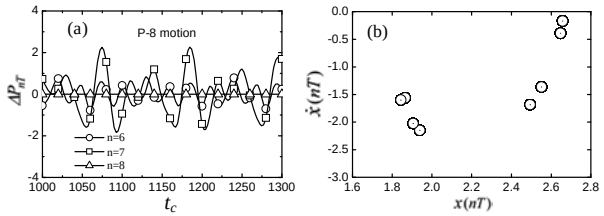

Fig. 7 Plots of ΔP_{nT} integration (left) and Poincaré map (right) with $f = 14.35$.

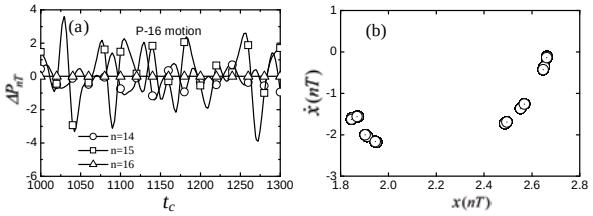

Fig. 8 Plots of ΔP_{nT} integration (left) and Poincaré map (right) with $f = 14.38$.

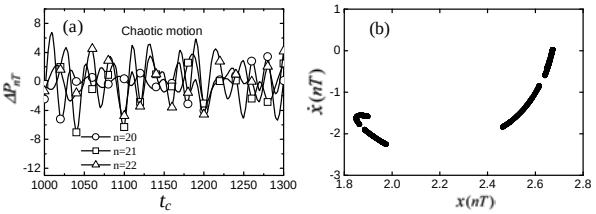

Fig. 9 Plots of ΔP_{nT} integration (left) and Poincaré map (right) with $f = 14.45$.

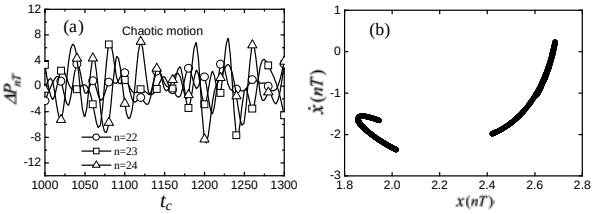

Fig. 10 Plots of ΔP_{nT} integration (left) and Poincaré map (right) with $f = 14.55$.

3.4 The effect of damping and stiffness parameters analysis

Damping is also one of the main factors affecting dynamic characteristics of nonlinear systems. Bifurcation diagrams shown in Fig. 11 was plotted in the form of P_T integration to be as a function of the f with the variation of damping parameter c_1. In the range $3.0 < f < 7.0$, the bifurcations of the system are illustrated for damping parameters c_1 of 0.55, 0.60, 0.70 and 0.75. As obvious from bifurcation responses shown in Fig. 11, increasing c_1 can reduce the response amplitude and narrows the chaotic zone. It is further observed that as the value of c_1 is increased from 0.55 to 0.60, the chaotic zone, where f is varied in the range $5.6 < f < 6.1$, gradually disappear. For the case of $c_1 = 0.70$, the chaotic zone in the half-left interval, i.e., $4.3 < f < 4.8$ was also narrowed in Fig. 11(c). For the case of $c_1 = 0.75$ in particular, the chaotic zones entirely disappear in Fig. 11(d). It can be seen that the system represents the complex dynamic characters at different damping coefficients

obviously. The chaotic zones gradually disappear when the damping parameter is increased. This feature indicates that the damping effect is relatively sensitive to the dynamic responses of a system. The effect of changing stiffness parameter is also investigated in this paper.

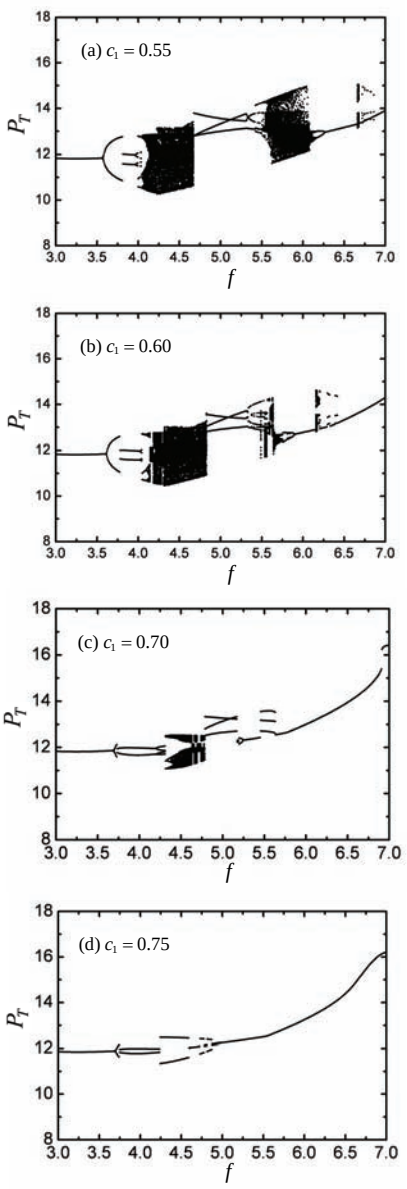

Fig. 11 Effect of damping coefficient, c_1 on the system responses of bifurcation diagrams using the response integration method with $c_2 = -1.0$, $c_3 = -1.0$, $k_1 = 0.08$, $k_2 = 0.65$, $k_3 = 0.26$, $\omega = 1.0$.

Bifurcation diagrams shown in Fig. 12 was plotted in the form of P_T integration to be as a function of the f with various stiffness parameters k_1. For a lower stiffness value of $k_1 = 0.08$, it is clearly seen that there are several chaotic regions occur in the ranges $3.66 < f < 4.17$, $4.55 < f < 5.76$, $6.31 < f < 6.38$ and $6.46 < f < 7.0$. As obvious from bifurcation responses shown in Fig. 12, increasing k_1 also reduces the response amplitude and narrows the chaotic zone. It is observed that as the value of k_1 is increased from 0.08 to 0.36, the chaotic zones gradually decrease. When k_1 increases further, at $k_1 = 0.52$ as shown in Fig. 12(c), the chaotic regions are found to turn into two from three. Then, with further variations of k_1, Fig. 12(d) shows that the chaotic zones disappear and the level of vibration is lower when the stiffness is larger (at $k_1 = 0.75$).

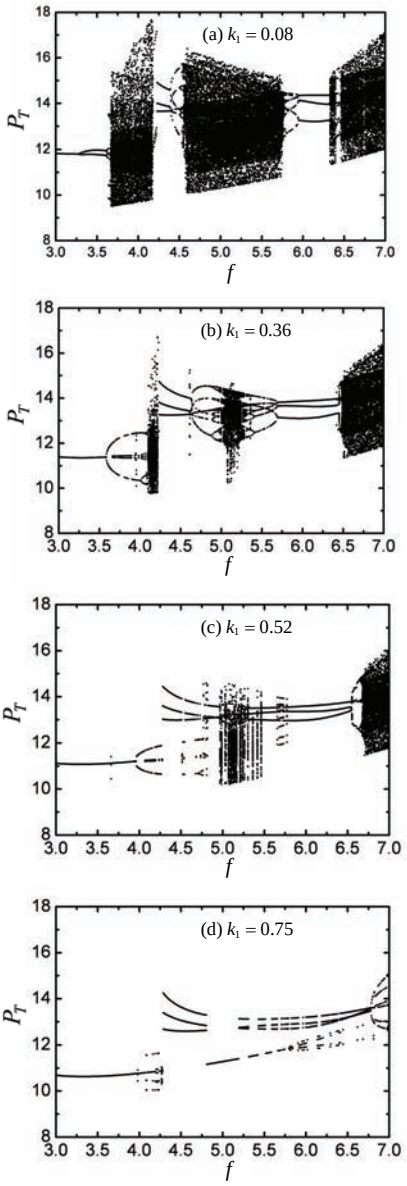

Fig. 12 Effect of stiffness coefficient, k_1 on the system responses of bifurcation diagrams using the response integration method with $c_1 = 0.15$, $c_2 = -1.0$, $c_3 = -1.0$, $k_2 = 0.65$, $k_3 = 0.26$, $\omega = 1.0$.

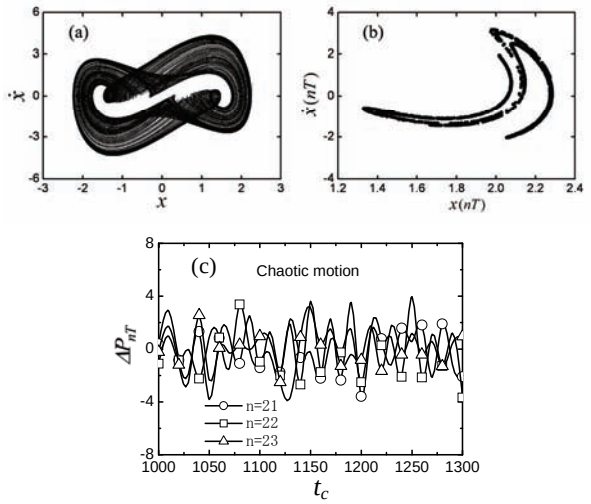

Fig. 13 Phase portrait, Poincaré map and ΔP_{nT} integration plot for $c_1 = 0.55$.

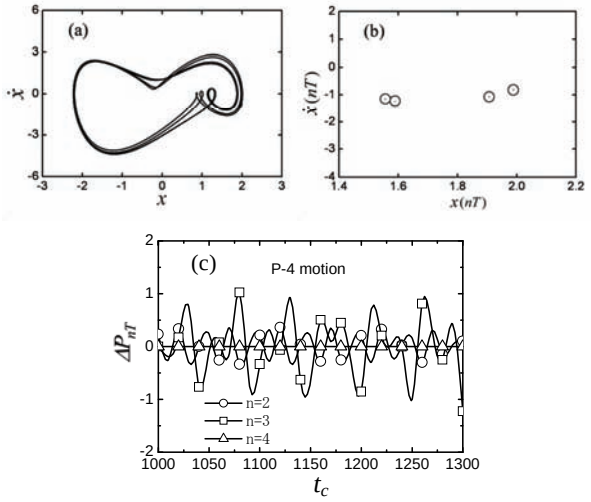

Fig. 14 Phase portrait, Poincaré map and ΔP_{nT} integration plot for $c_1 = 0.70$.

Figs. 13-14 show the phase portrait, the Poincaré map and the plots of ΔP_{nT} integration with various damping parameters, $c_1 = 0.55$ and $c_1 = 0.70$. In these calculations, we choose the other parameters as the same with Fig. 11. The chaotic motion was plotted for $c_1 = 0.55$ and the periodic motion for $c_1 = 0.70$. When $c_1 = 0.55$, the phase portrait also shows irregular motion as shown in Fig. 13(a). There are strange attractors representing chaotic motion in the Poincaré map as shown in Fig. 13(b). Furthermore, the ΔP_{nT} integration values never keep zero as continuously varying t_c even with the integration interval set very large ($n = 23$) as shown in Fig. 13(c). It indicates that responses are not periodic motions. When $c_1 = 0.70$, the motion is regular and periodic as the phase portrait shown in Fig. 14(a). There is four points in the Poincaré map as shown in Fig. 14(b). Therefore, the system response is a period-four motion. The result is the same as the plot of ΔP_{nT} integration as shown in Fig. 14(c).

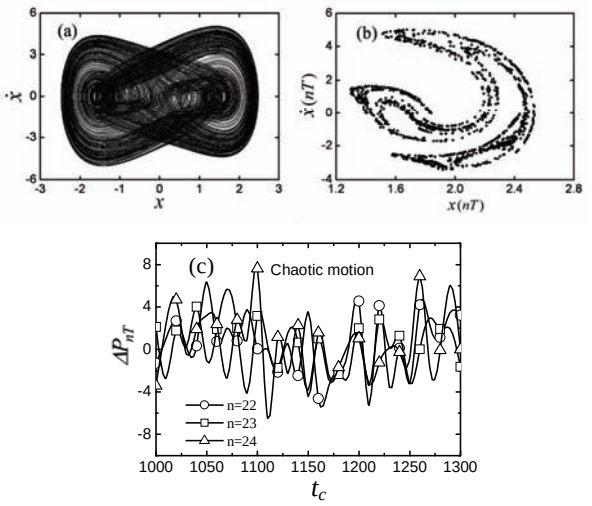

Fig. 15 Phase portrait, Poincaré map and ΔP_{nT} integration plot for $k_1 = 0.08$.

Figs. 15-16 show the phase portrait, the Poincaré map and the plots of ΔP_{nT} integration with various damping parameters, $k_1 = 0.08$ and $k_1 = 0.36$. In these calculations, we choose the other parameters as the same with Fig. 12. When $k_1 = 0.08$, the phase portrait also shows irregular motion as shown in Fig. 15(a). The chaotic response keeps active. As observed from Figs. 15(b), the results of the Poincaré section method also show the responses to be chaotic motion. At this time, it is found that the ΔP_{nT} integration values never keep zero as continuously varying t_c even with the integration interval set very large ($n = 24$) as shown in Fig. 15(c). When $k_1 = 0.36$, It can be seen from the Figs. 16(a) and 16(b) that the system vibration is period-three motion. The result is the same as the plot of ΔP_{nT} integration as shown in Fig. 16(c). This feature indicates that the stiffness effect is relatively sensitive to the dynamic responses of a nonlinear system. From above results, it is concluded that the stiffness and damping of the system can effectively suppress chaotic vibration and reduce vibration amplitude.

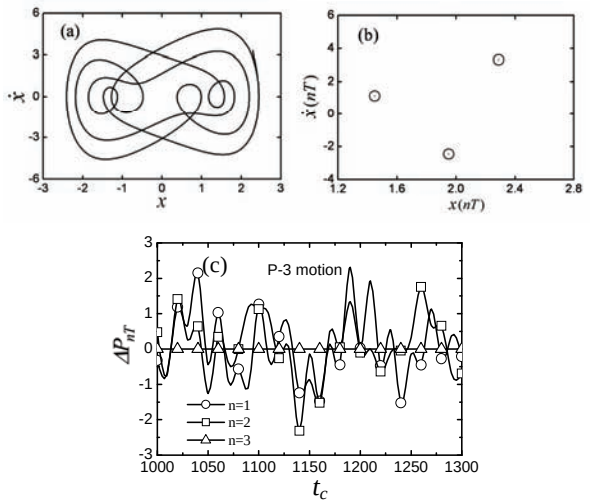

Fig. 16 Phase portrait, Poincaré map and ΔP_{nT} integration plot for $k_1 = 0.36$.

4 Conclusions

This study proposes the response integration algorithm to analyze the vibration responses of a Duffing-Van der Pol oscillator with periodic excitation. This method numerically integrates the distance between state trajectory and the origin in the phase plane during a specific period. It provides a quantitative characterization of system responses and can replace the role of the traditional stroboscopic technique (Poincaré section method) to observe bifurcations and chaos of the nonlinear oscillators. Utilizing the P_{nT} - integral quantity analytical method, the periodic response of the system can be clearly and simply drawn. It is a very useful tool to observe vibration responses which generally cannot be easily distinguished from the time history, the phase portrait and the Poincaré map. Due to the signal response contamination of system, thus it is difficult to identify the high-order responses of the subharmonic motion because of the sampling points on Poincaré map too near each other. Even the system responses will be made misjudgments. The response integration method is used to analyze nonlinear system. When P_{nT} (or $\Delta P_{nT} = 0$) is a fixed constant, the system response is periodic motion according to the definition of the response integration method. Such characteristics can avoid the disturbances described above. Therefore, it is more advantageous to use this method for analysis regarding limited measuring data or numerical simulation.

In this paper we have inspected the ΔP_{nT} integration plot and P_T integration bifurcation diagram to identify responses of a nonlinear oscillator in some cases. Applying this method, the effects of the change in the stiffness and the damping coefficients on the vibration features are investigated. With variation of system parameters, such as damping, stiffness, whirling speed and external forcing amplitude, chaotic response can be observed, along with other complex dynamics such as period- doubling bifurcation in the response. The numerical simulated results show that the response integration technique will be available to observe bifurcations and chaos of the nonlinear oscillator effectively and can precisely identify high-order subharmonic motion. By applying our proposed method and combining with the GA method, the control and synchronization of chaos in nonlinear dynamical systems are also interesting topics for future studies.

Acknowledgements

This work had supported by the National Science Council of R.O.C. with grant No. NSC-92-2212-E-033-016 and R&D Center for Membrane Technology in CYCU due to the center-of-excellence program from the Ministry of Education of R.O.C.

References:

[1] Thompson, J. M. T., Stewart H. B., *Nonlinear dynamics and chaos*, Chichester: Wiley; 1986.

[2] Leung, A. Y. T., and Fung, T. C., Construction of Chaotic Regions, *Journal of Sound and Vibration*, Vol. 86, 1989, pp. 445-455.

[3] Jackson, E. A., *Perspectives of Nonlinear Dynamics*, Cambridge University Press, New York, 1991.

[4] Holmes , J., P., *Nonlinear Oscillation and Bifurcation of Vector Fields*, Springer, New York, 1993.

[5] Lakshmanan, M., and Murali, K., *Chaos in Nonlinear Oscillators: Controlling and Synchronization*, World Scientific, Singapore, 1996.

[6] Lei, Y. M., and Xu, W., Chaos control by harmonic excitation with proper random phase, *Chaos, Solitons & Fractals*, Vol. 21, 2004, pp. 1175-1181.

[7] Kyprianidis, I. M., Volos, Ch. K. and Stouboulos, I. N., Suppression of chaos by linear resistive coupling, *WSEAS Trans. on Circuits and Systems*, Vol. 4, 2005, pp. 527-534.

[8] Parlitz, U., and Lauterborn, W., Period-Doubling Cascades and Devil's Staircases of

the Driven Van der Pol Oscillator, *Physical Review A*, Vol. 36**,** 1987, pp. 1428-1434.

[9] Dooren, R. V., and Janssen, H., A Continuation Algorithm for Discovering New Chaotic Motion in Forced Duffing Systems, *Journal of Computational and Applied Mathematics*, Vol. 66**,** 1996, pp. 527-541.

[10] Xu, J. X., and Jiang, J., The global bifurcation characteristics of the forced Van der Pol oscillator, *Chaos, Solitons & Fractals*, Vol. **7,** 1996, pp. 3-19.

[11] Aguirre, J., and Sanjuán, M. A. F., Unpredictable behavior in the Duffing oscillator: Wada basins, *Physica D*, Vol. 171, 2002, pp. 41–51.

[12] Acho L., Rolon, J. and Benitez, S. A., Chaotic oscillator using the Van der Pol dynamic immersed into a jerk system. *WSEAS Trans. on Circuits and Systems*, Vol. 3, 2004, pp. 198–199.

[13] Qun He, Wei Xu, Haiwu Rong, Tong Fang, Stochastic bifurcation in Duffing-Van der Pol oscillators, *Physica A* , Vol. 338, 2004, pp. 319-334.

[14] Hong, L. and Xu, J., A Chaotic Crisis between Chaotic Saddle and Attractor in Forced Duffing Oscillators, *Communication in Nonlinear Science and Numerical Simulation*, Vol. 9, 2004, pp. 313-329.

[15] Jing, L., and Wang, R., Complex dynamics in Duffing system with two external forcings, *Chaos, Solitons and Fractals*, Vol. 23, 2005, pp. 399-411.

[16] Volos, Ch. K., Kyprianidis, I. M. and Stouboulos,, I. N., Synchronization of Two Chaotic Duffing-type Electrical Oscillators, *Proceeding 10th WSEAS International Conference on Circuits and Systems*, 2006, pp.179-184.

[17] Kim, Y., Lee, S. Y., and Kim, S. Y., Experimentally observation of dynamic stabilization in a double-well Duffing oscillator, *Physics Letters A*, Vol. **275,** 2000, pp.254-259.

[18] Kakmeni, F. M. M., Bowong, S., Tchawoua, C., and Kaptouom, E., Strange attractors and chaos control in a Duffing-Van der Pol oscillator with two external periodic forces, *Journal of Sound and Vibration*, Vol. 277, 2004, pp. 783-799.